JOURNAL OF ELECTROMAGNETIC ENGINEERING AND SCIENCE, VOL. 24, NO. 3, 276~284, MAY. 2024

https://doi.org/10.26866/jees.2024.3.r.228
ISSN 2671-7263 (Online) · ISSN 2671-7255 (Print)

LCP-Based Low-Cost Base Station Antenna for 3.7 GHz 5G Band

Youngju Lee[1] · Seung-Ho Choi[2] · Bum-Hee Lee[2] · Jung-Yub Lee[2] · Jae Hee Kim[3,*]

Abstract

This paper presents a large-scale base station antenna assembly structure that is low-cost, reliable, and easy to manufacture. The antenna element is composed of a low-loss liquid crystal polymer based on a plastic molded module and a modified wideband stacked patch antenna. The base station antenna consists of a 4 × 8 antenna module, with each module comprising 3 × 1 subarrays along with dual-polarized antenna elements. The antenna element achieved an efficiency of 91% and an impedance bandwidth of 1.14 GHz within a height of 10 mm at 3.7 GHz. Furthermore, the fabricated array antenna structure was tested and verified to have an effective isotropic radiated power of 75.6 dBm at boresight and a steering range of less than ±60°. Therefore, the proposed structure meets the required antenna and beam-forming performance for commercial 5G active antenna systems.

Key Words: Base-Station Antenna, Liquid Crystal Polymer (LCP), Stacked Patch, 5G.

I. Introduction

The 5G wireless communication networks are considered suitable candidates for next-generation cellular systems owing to growing traffic in the existing 4G spectrum and demand for high data rates. Recently, 5G commercial services have been deployed in South Korea and the United States. In America, the provision of C-band services at 3.7–3.98 GHz is already underway, beginning with small-cell services in the millimeter wave band. In this context, to ensure a successful network equipment business, high-performance base stations that produce high yields need to be mass-produced at low cost.

For C-band services, massive multi-input multi-output (MIMO) is a major technology that has the potential to improve the reliabilities of data links as well as performances related to the capacity and user experience of 5G-enhanced mobile broadband using hundreds of large antenna arrays in a base station [1]. In particular, MIMO systems apply highly directed radiation beams through adaptive beamforming and signal processing algorithms to different pairs of antennas using active antenna systems (AASs) [2].

Notably, the passive antenna beam patterns in legacy cellular systems are fixed, and they are shaped to transmit signals uniformly within the coverage direction.

In contrast, AASs comprising multiple antenna elements can transmit and receive signals through beams with narrow beamwidths and high gains. In addition, such systems can adjust the amplitude and phase of each transmitted/received radio frequency chain to dynamically control the beam direction toward the location of the desired user, resulting in significant throughput and efficiency improvements [3].

Manuscript received June 12, 2023 ; Revised August 30, 2023 ; Accepted October 18, 2023. (ID No. 20230612-111J)
[1]Advanced Network Development Office, Electro-Materials Business, Doosan Corporation, Yongin, Korea.
[2]H/W Development Team, Network Business Division, Samsung Electronics, Suwon, Korea.
[3]School of Electrical, Electronics and Communication Engineering, KOREATECH, Cheonan, Korea.
[*]Corresponding Author: Jae Hee Kim (e-mail: jaehee@koreatech.ac.kr)

Fig. 1 presents an example of the antenna configuration of an active antenna system for a massive MIMO. In terms of the development cost and angular coverage of the cell, applying independent digital beamforming to every antenna element would be inefficient. Hence, a single transmit/receive chain, including a power amplifier and a low-noise amplifier, is connected to a group of antennas, called a subarray. The subarray consists of three antenna elements, with each antenna element having two polarizations—positive polarization (P pol.), which is tilted by +45° relative to the vertical axis, and negative polarization (N pol.), which is tilted by −45°. Since a signal input is necessary for each polarization, each subarray bears two input ports. Therefore, an entire array antenna comprises multiple subarrays as its array element. In particular, four vertical columns of subarrays and eight horizontal rows of subarrays create the entire array. Fig. 1(b) shows the configuration of a simple radio structure in AASs, which is connected to an antenna. The active antenna system is composed of 64 transceiver chains, each of which should deliver a precise and stable amplitude and phase to the antenna in various environments to create the desired beam-forming pattern. Furthermore, the calibration network serves to calibrate the amplitude and phase of the signal transmitted to the antenna.

In recent years, increasing demand for broadband dual-polarized antennas characterized by a compact and planar configuration has been observed, owing to their low cost, ease of manufacturing, and system integration. To address this demand, many dual-polarized base station antennas have been proposed to achieve broadband and dual-polarization performance, including antennas that involve modifying the dipole structure [4–6] and patch antennas using an L-probe feed and a meander line feed [7–11]. Notably, a double-layered stacked patch antenna has also been proposed in the literature for attaining a broad impedance band and flat gains [12]. Although these antennas exhibit broadband characteristics, they tend to have high antenna height and a mechanically complex structure—features that discourage mass production—since most of them have been produced with a focus on the performance of a single antenna element.

In this regard, liquid crystal polymers (LCPs) with low dielectric constant and low loss tangent have been proposed for use in circuit devices, module packaging, and flexible antenna arrays [13, 14]. Notably, LCPs are attractive materials for use in antennas due to their low water absorption and low dielectric losses.

In this paper, a novel low-profile, broadband, dual-polarized antenna structure is proposed for low cost and easy manufacturing of large-scale AASs for base stations. The proposed antenna is composed of 96 antenna elements with dimensions of 360 mm × 930 mm × 10 mm. Furthermore, a low-loss LCP-based plastic molding substrate is employed to easily fabricate a 3D fixture for the flexible 3D design of the antenna and feed line, as well as to reduce costs for fabricating two subarray-based molding modules compared to the costs involved in using a large-scale printed circuit board (PCB) substrate.

The proposed antenna operated efficiently in the C-band from 3.7 to 3.98 GHz. Furthermore, its performance was verified by comparing simulation results. The verification results confirmed that the novel plastic molding structure proposed in this study can be employed for the mass production of large-scale antennas, thus satisfying the cost reduction requirements as compared to antennas based on PCB.

II. 3 × 1 Subarray on Plastic Molded Module

A basic plastic molding antenna element for large-scale MIMO systems at 3.7 GHz is presented in Fig. 2. A single

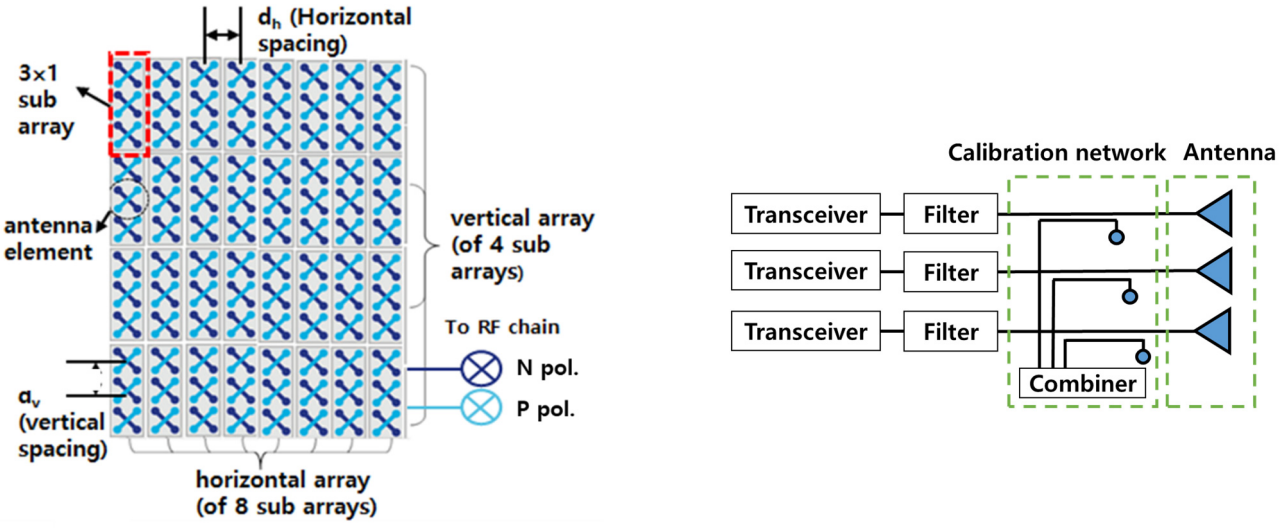

(a) (b)

Fig. 1. An example of active antenna systems for massive MIMO radio configuration: (a) array antenna and (b) a simple radio structure.

antenna element consists of two stacked patches—a lower patch and an upper patch—that are floated on a plastic molding substrate while maintaining a constant gap between the lower stacked L-shaped coupled feed. The stacked patches were used to obtain a wide impedance bandwidth, which was satisfied when the upper patch was sufficiently floated from the lower patch for loose coupling. Furthermore, two resonant frequencies were placed closely to achieve wideband impedance using a relatively thick antenna.

When the distance between the upper and lower patches was decreased to lower the height of the antenna, strong coupling was observed, resulting in a wider separation between the two resonance frequencies. This led to some frequency regions between the two resonance frequencies failing to meet $S_{11} < -10$ dB. To address this issue, this paper proposes a structure in which a slot is made in the lower patch to reduce coupling while also narrowing the distance between the upper and lower patches. The length and width (w_{up}) of the upper patch in Fig. 2(c) are 26 mm, while those (w_{low}) of the lower patch are 21 mm. Furthermore, the size (w_{slot}) of the hole in the lower patch is 11 mm. The upper patch and lower patch are located 10 mm and 6 mm above the ground, respectively, while the feed is placed 5 mm above the ground. The upper and lower patches are supported by a plastic mold while also keeping an air gap between the patches. The feed line is raised 12 mm away from the center of the antenna, with the length of the feed line coupled with the lower patch being 5 mm.

The LCP material, which was used as the primary material for constructing the plastic structure, acted as a position fixture, as well as the substrate of the antenna and the feed line. This material was chosen because it allowed relatively easy fabrication of molding for mass production, was characterized by good thermal management in the molding process, and exhibited low loss characteristics for high radio frequency (RF) performance, such as insertion loss and antenna efficiency, as shown in Table 1.

Table 1. Comparison of various types of materials for the molded module

Material	Permittivity	Loss tangent	HDT (°)	Price
DS-7409	3.2	0.0025	400	High
LCP	3.7	0.0023	305	Mid.
PPS	4.1	0.0045	270	Mid.
PC	2.7	0.012	130	Low

LCP = liquid crystal polymer, PPS = polyphenylene sulfide, PC = poly carbonates, HDT = heat deflection temperature.

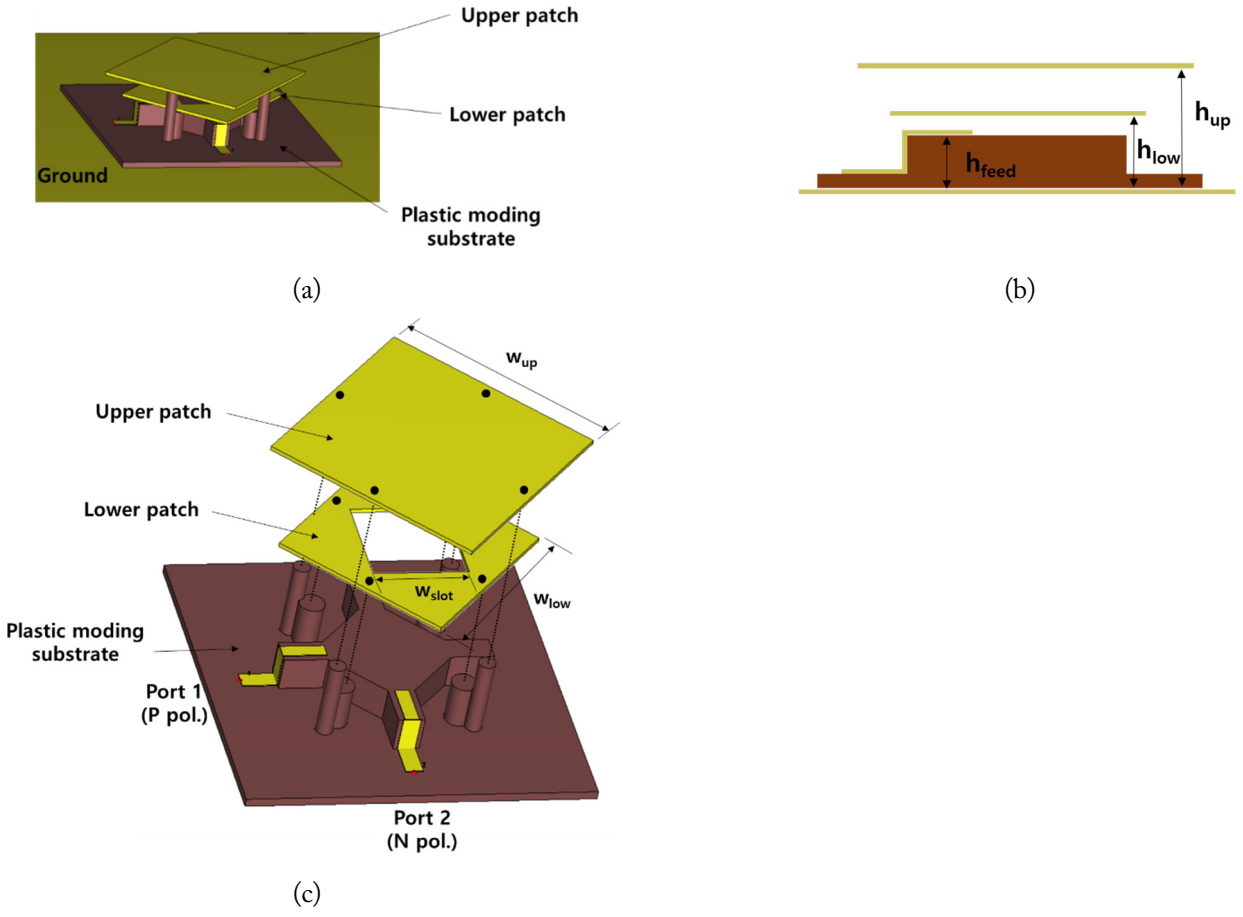

Fig. 2. Structure of the proposed antenna element: (a) 3D view, (b) side view, and (c) each part of the antenna structure.

Furthermore, compared to conventional fabrication processes based on large-scale PCBs for large-sized antennas, the proposed module has a relatively small size and could be repeatedly assembled on the metal ground to from a large-scale antenna.

In the absence of a hole ($w_{slot} = 0$) in the lower patch of the structure depicted in Fig. 2, the input impedance is simulated based on the height of the upper patch. Fig. 3(a) shows a Smith chart, while Fig. 3(b) depicts the magnitude of S_{11} with respect to frequency. It is evident that as the height of the upper patch increases, the coupling between the upper and lower patches decreases, ultimately leading to a reduction in the size of the resonance circle formed on the Smith chart. Additionally, the second resonant frequency declines as the coupling decreases. When the two resonance frequencies are located close to each other, an $S_{11} < -10$ dB is obtained over the entire frequency band. Therefore, although increasing the height of the upper patch is favorable from the perspective of bandwidth, it results in the disadvantage of thickening the antenna.

To reduce coupling without increasing the thickness of the antenna, a hole was introduced in the lower patch. The simulated S_{11} values when using varying hole sizes (w_{slot}) for the same antenna structure as in Fig. 2 are presented in Fig. 4. As shown in Fig. 4(a), an increase in hole size leads to a decrease in coupling, resulting in a smaller resonant circle on the Smith chart. Additionally, Fig. 4(b) shows that the second resonant frequency also declines as the hole size increases. This indicates that the introduction of holes in the lower patch results in reduced coupling with the upper patch without having to increase its height. The shift in the position of the resonance circle on the Smith chart occurs because increasing the hole size in the lower patch leads to a lowering of the patch's resonant frequency. In this context, impedance matching and other related factors can also be optimized by adjusting the length of the L-probe. The S_{11} of the proposed antenna is traced by the blue dash-dotted line in Fig. 4, achieving a 1.14 GHz (3.32–4.46 GHz) impedance bandwidth.

Fig. 5 illustrates the simulated realized gain in terms of different frequencies. Within the impedance bandwidth of 3.32–4.46 GHz, the antenna gain varies between a minimum of 8.1 dBi and a maximum of 9.5 dBi. Moreover, the antenna gain over various frequencies reveals considerable wideband performance for a single element.

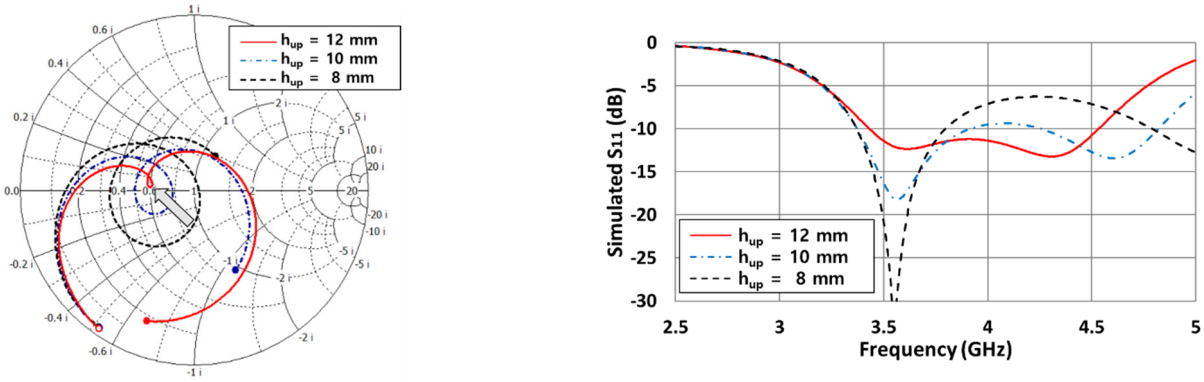

(a) (b)

Fig. 3. Simulated S_{11} of the antenna element for different heights of the upper patch; (a) Smith chart and (b) magnitude in dB.

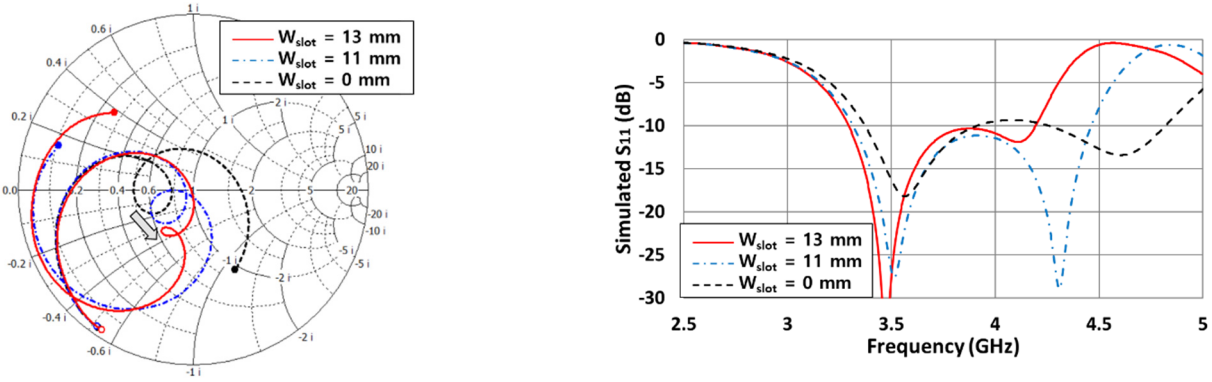

(a) (b)

Fig. 4. Simulated S_{11} of the antenna element for different hole sizes of the lower patch; (a) Smith chart and (b) magnitude in dB.

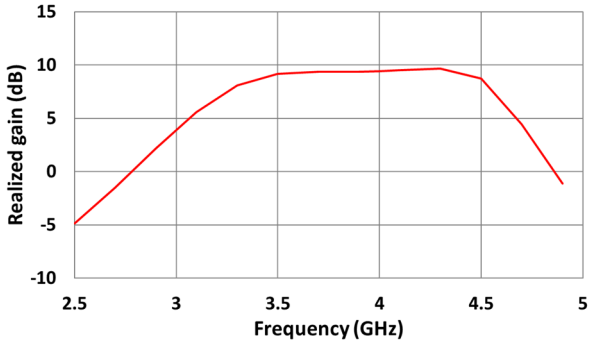

Fig. 5. Simulated realized gain of the antenna element.

To enrich the distribution of the radiated power within the coverage area and to reduce interference from the upper region, a 6° electronically down-tilt beam is required in the vertical direction of the base station antenna. For a 6° down-tilt beam in the vertical direction, the phase difference at each feed network for a subarray should be about 36°. Notably, a 3 × 1 subarray in the vertical direction would be more efficient than using three single antennas for independent digital beamforming and RF chains even the vertical beamforming range of the antenna is limited to a specified range.

When determining the distance between the vertical antennas, the vertical beamforming range and increment of gain should be carefully considered as the main specifications of the active antenna system. For the system proposed in this study, the distance between antennas in the vertical direction was 0.78λ (61 mm) for a vertical scan range of 20° and a gain of approximately 11 dBi. Meanwhile, the distance between antennas in the horizontal direction was 0.54λ (42 mm). Notably, a 3 × 1 subarray can support two polarizations—P pol. and N pol. Therefore, two signal lines supporting these two polarizations of the 3 × 1 subarray antenna were connected using the transmit/receive RF chain.

The size of the module, composed of two 3 × 1 subarrays, was determined by accounting for the productivity of the molding process and the efficiency of assembling it on metal ground. Furthermore, the 3 × 1 feed lines were created by cutting aluminum sheets of 100 μm thickness, which were then attached to the plastic fixture using specific melting structures, as shown in Fig. 6.

Fig. 7 shows the simulated *S*-parameters of the two 3 × 1 subarrays. S(N1,N1) refers to the S_{11} of the N pol. port, while S(P1,P1) denotes the S_{11} of the P pol. port. Furthermore, S(N1,N2) refers to the co pol. isolation between ports N1 and N2, while S(N1,P1) is the self-cross pol. isolation between ports N1 and P1. Finally, S(P1,N2) indicates the cross-pol. isolation between ports P1 and N2. The S_{11} of the two polarizations sat-

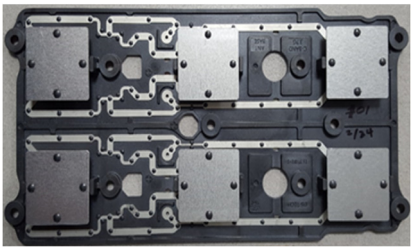

(a)

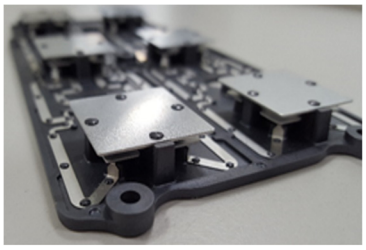

(b)

(c)

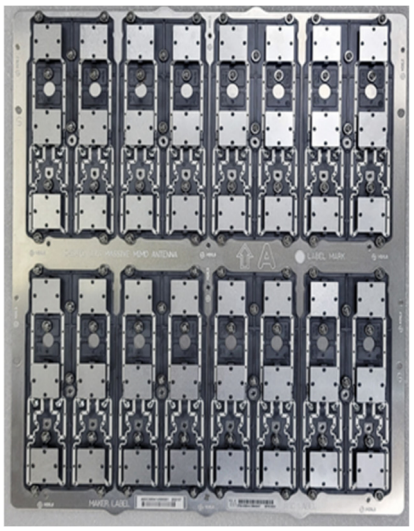

(d)

Fig. 6. Fabricated plastic molded antenna module: (a) top view of the two 3 × 1 subarrays, (b) side view of the subarray, (c) top view of the antenna element without the upper and lower patches, and (d) half of the total antenna array structure.

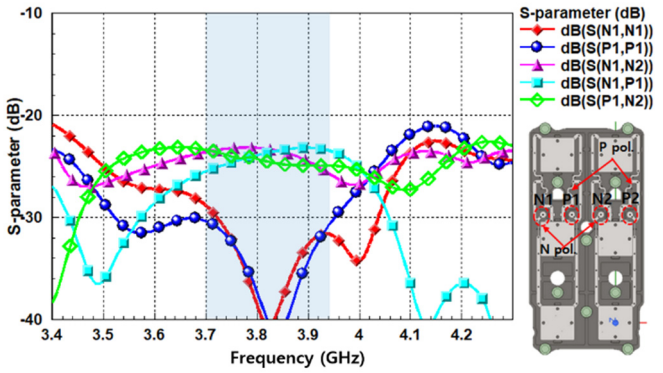

Fig. 7. Simulated *S*-parameters of the two 3 × 1 subarrays.

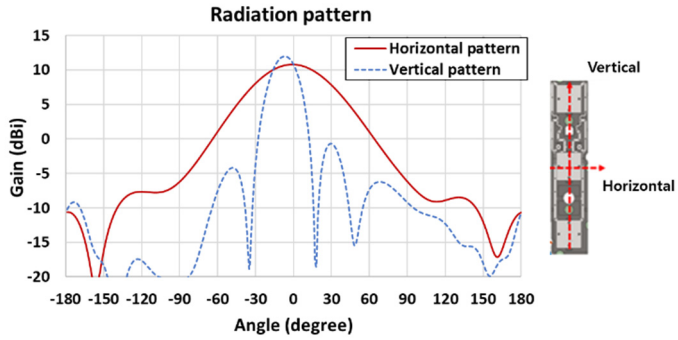

Fig. 8. Simulated radiation patterns of the 3 × 1 subarray antenna.

isfied the −20 dB specification and port isolation. Furthermore, polarization isolation between the two ports of the antennas was at least under −21 dB within the concerned frequency band. Notably, the broader impedance bandwidth achieved by the sub-array antenna compared to a single antenna can be attributed to the influence of the feeding structure.

Fig. 8 traces the simulated antenna patterns of the 3 × 1 subarray supporting P pol. Notably, the pattern of N pol. was found to be similar to that of P pol., since the feeding point was structurally symmetric. Furthermore, the 3 dB beamwidth of the horizontal pattern was approximately 61°, while the gain of the subarray was 10.7 dBi. Similarly, the 3 dB beamwidth of the vertical pattern was 20° with a 6° fixed down-tilt angle, while the peak gain was 11.7 dBi. This indicates that the scanning range of the entire active antenna system can be accurately estimated from the subarray beam pattern.

III. Radiation Patterns of the Active Antenna System

Each input port of the subarray antenna was connected to beamforming integrated circuits (ICs). A user-specific beam was transmitted toward the individual receive antenna of the user through a beamforming weight vector, defined as a steering vector toward the user's direction in line-of-sight (LOS) conditions or a maximal ratio transmission vector in non-LOS environments. In LOS conditions, the array gain was observed to be equal to the number of subarrays. The maximum antenna gain of the user-specific beam can be expressed in dB as the sum of its array factor and the subarray gain. Notably, the array factor is usually proportional to the number of subarrays in an array, while the subarray gain is approximately proportional to the number of antenna elements within a subarray (3 × 1 subarray) and the spacing between adjacent subarrays (4 × 8 system). The antenna gain toward the boresight of the proposed active antenna system was estimated to be approximately 25.7 dBi when considering two factors—gains of the array factor (15 dB) and the subarray (10.7 dBi). Fig. 9 shows the simulated and measured patterns of the user-specific beam of the proposed active antenna system at boresight, exhibiting maximum gain in the azimuth and vertical directions at 3.7 GHz. The 3 dB beamwidth was approximately 12° in the azimuth direction and 5° in the vertical direction. Notably, the measured beam pattern and gain were similar to the simulation results obtained at boresight. The antenna efficiency was almost above 91%, including the feedline loss from a low-loss LCP-based substrate.

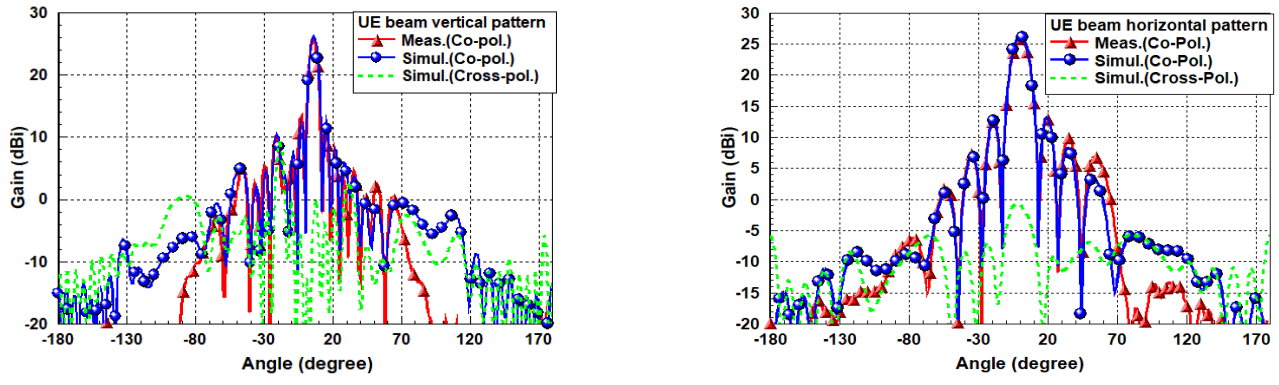

(a) (b)

Fig. 9. Radiation patterns of the user-specific beam: (a) horizontal pattern and (b) vertical pattern.

The set-level, user-specific beam performance of the proposed active antenna system with maximum tilting range in the azimuth and elevation axes was measured, as shown in Fig. 10. The measured peak effective isotropic radiated power (EIRP) was 75.6 dBm, while the scanning range was 120° from −60° to 60° in the azimuth axis. The tilting range was approximately 20°—from +16° down-tilt angle to −4° up-tilt angle—along with the 6° fixed-tilt angle achieving maximum gain in the vertical axis. The cross-polarization ratio level—the ratio between co-polarization and cross-polarization—was 30.2 dB at boresight and 13.5 dB at the 60° scanning angle. Therefore, the beamforming performance of the proposed structure, including the performance of the system elements, such as antennas, RF transceivers, and other related functions, can be expected to satisfy the beamforming performance of commercial base stations.

Table 2 compares the performance of the antenna proposed in this paper with existing references [7–9, 15–18]. It is observed that the resonance frequency of the references is below 2 GHz, while their antennas were designed with a height of at least 17 mm. Additionally, while antennas designed for the 3.7 GHz band has a lower height compared to the proposed antenna, they still fail to reach a bandwidth as wide as that attained in this paper.

IV. Conclusion

This study investigated a novel low-cost antenna fabrication and assembly solution for large-scale AASs. The proposed antenna comprises over 96 antenna elements at 3.7 GHz, and involves repeatedly assembling an LCP-based plastic module using an attachable 3 × 1 feed line. In addition, a low-profile wideband antenna with stacked patch antennas was obtained, even with loose coupling between the upper and lower patch antennas, by perforating the inner patch antenna. Subsequently, the proposed structure was verified to satisfy a wide impedance bandwidth of 1.14 GHz within a height of 10 mm. Furthermore, set-level beamforming measurements of the active antenna system with 64-chain (4 × 8 array and two pol.) transceivers were verified, exhibiting a maximum EIRP of 75.5 dBm at boresight and a steering range of <±60° in the azimuth axis. Overall, the proposed solution can be considered a suitable candidate for use in commercial active antenna system-based base stations with large-scale arrays at 3.7 GHz.

The simulations and analyses conducted in this paper were supported by the 2022 Education and Research promotion program of KOREATECH.

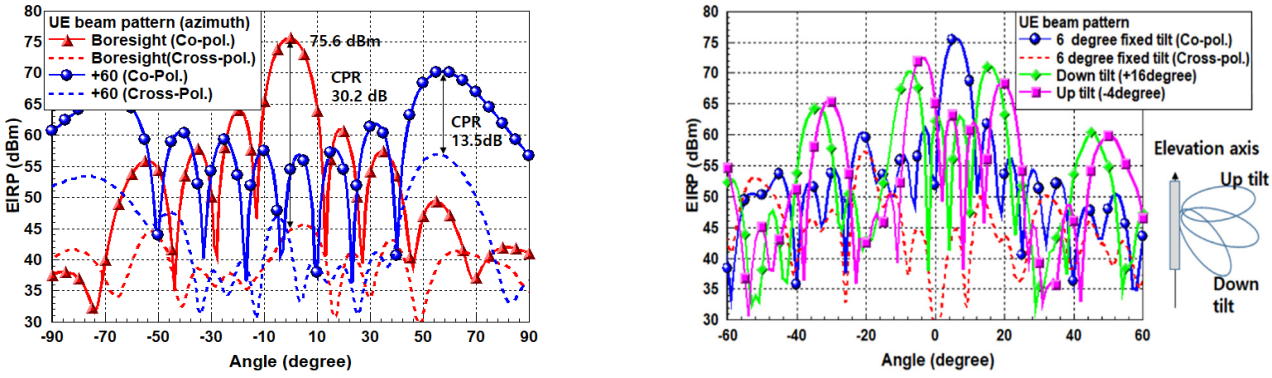

(a) (b)

Fig. 10. Scanned patterns of the user-specific beam: (a) horizontal pattern (azimuth axis) and (b) vertical pattern (elevation axis).

Table 2. Comparison of the proposed antenna performance with that of existing references

	Antenna type	Frequency (GHz)	Height (mm)	Bandwidth (GHz)
Wong et al. [7]	L-probe single patch	1.8	17	0.43
Lai and Luk [8]	Meandering probe single patch	1.9	17.5	0.43
Guo et al. [9]	L-probe single patch	2.0	22.4	0.67
Zheng and Chu [15]	Loop-dipole	2.0	35	1.15
Nie et al. [16]	Slotted patch with shorting strips	2.0	40	1.18
Huang et al. [17]	Stacked patch	3.7	8.7	0.40
Gao et al. [18]	Slot patch	3.7	7.8	0.40
This work	L-probe stacked patch with hole	3.7	10	1.14

REFERENCES

[1] E. G. Larsson, O. Edfors, F. Tufvesson, and T. L. Marzetta, "Massive MIMO for next generation wireless systems," *IEEE Communications Magazine*, vol. 52, no. 2, pp. 186-195, 2014. https://doi.org/10.1109/MCOM.2014.6736761

[2] K. N. Poudel and W. Robertson, "Metamaterial inspired antenna design for massive MIMO, 5G communications system," in *Proceedings of 2017 USNC-URSI Radio Science Meeting (Joint with AP-S Symposium)*, San Diego, CA, USA, 2017, pp. 103-104. https://doi.org/10.1109/USNC-URSI.2017.8074918

[3] W. Roh, J. Y. Seol, J. Park, B. Lee, J. Lee, Y. Kim, J. Cho, K. Cheun, and F. Aryanfar, "Millimeter-wave beamforming as an enabling technology for 5G cellular communications: theoretical feasibility and prototype results," *IEEE Communications Magazine*, vol. 52, no. 2, pp. 106-113, 2014. https://doi.org/10.1109/MCOM.2014.6736750

[4] B. Q. Wu and K. M. Luk, "A broadband dual-polarized magneto-electric dipole antenna with simple feeds," *IEEE Antennas and Wireless Propagation Letters*, vol. 8, pp. 60-63, 2008. https://doi.org/10.1109/LAWP.2008.2011656

[5] Y. Gou, S. Yang, J. Li, and Z. Nie, "A compact dual-polarized printed dipole antenna with high isolation for wideband base station applications," *IEEE Transactions on Antennas and Propagation*, vol. 62, no. 8, pp. 4392-4395, 2014. https://doi.org/10.1109/TAP.2014.2327653

[6] Y. Cui, R. Li, and P. Wang, "A novel broadband planar antenna for 2G/3G/LTE base stations," *IEEE Transactions on Antennas and Propagation*, vol. 61, no. 5, pp. 2767-2774, 2013. https://doi.org/10.1109/TAP.2013.2244837

[7] H. Wong, K. L. Lau, and K. M. Luk, "Design of dual-polarized L-probe patch antenna arrays with high isolation," *IEEE Transactions on Antennas and Propagation*, vol. 52, no. 1, pp. 45-52, 2004. https://doi.org/10.1109/TAP.2003.822402

[8] H. W. Lai and K. M. Luk, "Dual polarized patch antenna fed by meandering probes," *IEEE Transactions on Antennas and Propagation*, vol. 55, no. 9, pp. 2625-2627, 2007. https://doi.org/10.1109/TAP.2007.904158

[9] Y. X. Guo, K. W. Khoo, and L. C. Ong, "Wideband dual-polarized patch antenna with broadband baluns," *IEEE Transactions on Antennas and Propagation*, vol. 55, no. 1, pp. 78-83, 2007. https://doi.org/10.1109/TAP.2006.888398

[10] I. Kim and B. Lee, "Wideband antenna for high-frequency 5G wireless communication," *Journal of Electromagnetic Engineering and Science*, vol. 22, no. 3, pp. 296-301, 2022. https://doi.org/10.26866/jees.2022.3.r.90

[11] J. Cho, T. H. Lim, Y. Kim, and H. Choo, "Design of a wideband printed patch dipole antenna with a balanced on-board feeding network," *Journal of Electromagnetic Engineering & Science*, vol. 22, no. 6, pp. 631-637, 2022. https://doi.org/10.26866/jees.2022.6.r.132

[12] K. Ding, Y. Wu, K. H. Wen, D. L. Wu, and J. F. Li, "A stacked patch antenna with broadband circular polarization and flat gains," *IEEE Access*, vol. 9, pp. 30275-30282, 2021. https://doi.org/10.1109/ACCESS.2021.3059948

[13] Z. Zhou, W. Li, J. Qian, W. Liu, Y. Wang, X. Zhang, et al., "Flexible liquid crystal polymer technologies from microwave to terahertz frequencies," *Molecules*, vol. 27, no. 4, article no. 1336, 2022. https://doi.org/10.3390/molecules27041336

[14] G. DeJean, R. Bairavasubramanian, D. Thompson, G. E. Ponchak, M. M. Tentzeris, and J. Papapolymerou, "Liquid crystal polymer (LCP): a new organic material for the development of multilayer dual-frequency/dual-polarization flexible antenna arrays," *IEEE Antennas and Wireless Propagation Letters*, vol. 4, pp. 22-26, 2006. https://doi.org/10.1109/LAWP.2004.841626

[15] D. Z. Zheng and Q. X. Chu, "A multimode wideband $\pm$ 45° dual-polarized antenna with embedded loops," *IEEE Antennas and Wireless Propagation Letters*, vol. 16, pp. 633-636, 2016. https://doi.org/10.1109/LAWP.2016.2594240

[16] L. Y. Nie, X. Q. Lin, Y. J. Chen, J. Zhang, B. Wang, Z. Q. Yang, and Y. Fan, "A low-profile coplanar dual-polarized and dual-band base station antenna array," *IEEE Transactions on Antennas and Propagation*, vol. 66, no. 12, pp. 6921-6929, 2018. https://doi.org/10.1109/TAP.2018.2869222

[17] W. Huang, Y. He, W. Li, L. Zhang, S. W. Wong, and Z. Zeng, "A low-profile dual-polarized wideband antenna for 5G massive MIMO base station," in *Proceedings of 2021 IEEE International Workshop on Electromagnetics: Applications and Student Innovation Competition (iWEM)*, Guangzhou, China, 2021, pp. 1-3. https://doi.org/10.1109/iWEM53379.2021.9790399

[18] X. Gao, L. Zhang, Y. He, L. Zhang, W. Li, S. W. Wong, and C. H. Liao, "A dual-polarized compact patch antenna for sub-6 GHz 5G base stations," in *Proceedings of 2020 IEEE Asia-Pacific Microwave Conference (APMC)*, Hong Kong, 2020, pp. 752-754. https://doi.org/10.1109/APMC47863.2020.9331429

Young Ju Lee
https://orcid.org/0000-0001-5004-8238

is currently the vice president of the Advanced Network Development Office at Doosan Corporation, South Korea, where he is involved in the research of mmWave antenna modules for 5G and advanced communications. From 2005 to 2018, he was a project leader with Samsung Electronics, South Korea, where he focused on 5G antenna systems in the sub-6 GHz and mmWave bands. His research interests include the design of beamforming array antennas for 5G communication systems, analysis of indoor and outdoor propagation for channel modeling, and mobile and base station antenna applications using electromagnetic wave technology. He received his doctorate in Electronics and Electrical Engineering from Pohang University of Science and Technology (POSTECH), Pohang, Korea, in 2005.

Seung-Ho Choi
https://orcid.org/0000-0001-9387-4855

received his Ph.D. degree from the School of Electrical Engineering at Korea University, Seoul, Korea, in 2018. He is currently working as an antenna engineer at Samsung Electronics, Korea. His research interests include sub-6 GHz antennas and phase shifters for 5G base stations.

Bum-Hee Lee
https://orcid.org/0009-0001-4971-5010

received his B.S. degree in radio wave engineering from Chungnam National University, Daejeon, Korea, in 2018. He is currently working as an antenna engineer at Samsung Electronics, Korea. His research interests include massive MIMO antenna arrays and sub-6 GHz antennas for 5G base stations.

Jung-Yub Lee
https://orcid.org/0009-0006-2487-6033

is currently working with Samsung Electronics, where he is responsible for the research of antenna technologies for 5G communications. His research interests include the design of beamforming array antennas for various communication systems as well as mobile and base station applications using electromagnetic wave technology. He received his Ph.D. degree from the Department of Electrical Engineering at Seoul National University, Seoul, Korea, in 2007.

Jae Hee Kim
https://orcid.org/0000-0003-2193-928X

received his B.S. degree in electrical engineering from Korea University, Seoul, Korea, in 2005, and his Ph.D. degree in electrical engineering from Pohang University of Science and Technology, Pohang, Korea, in 2010. From 2010 to 2012, he worked as a senior engineer with Samsung Electronics, Suwon, Korea. From 2012 to 2020, he was a senior researcher at the Korea Railroad Research Institute in Uiwang, South Korea. He is currently an associate professor at the School of Electrical, Electronics, and Communication Engineering, Korea University of Technology and Education, Cheonan, Korea. His research interests include the design and analysis of antennas and microwave components, and the development of wireless power transfer systems for railways.